Coexistence of Multi-Dimensional Chirp Spread Spectrum in Underwater Acoustic Networks

Kerem Enhos, Emrecan Demirors, Deniz Unal, Tommaso Melodia
Institute for the Wireless Internet of Things, Northeastern University, Boston, MA 02115
USA Email: {enhos.k, e.demirors, unal.d, melodia}@northeastern.edu

ABSTRACT

Most underwater acoustic networks lack standard communication protocols, which leads communication nodes to operate in heterogeneous networks using physical layers. This exposes challenges to efficient spectrum allocation and channel utilization in large-scale underwater networks. To address these challenges, Multi-Dimensional Chirp Spread Spectrum (MCSS) is proposed as a physical layer that enables robust and efficient communication under the interference of unregulated physical layers in a heterogeneous network manner. Usage of MCSS offers zero signaling exchange among the coexisting technologies while maintaining successful communication and cooperative information rate increase. We first evaluated the performance of the proposed communication scheme in a heterogeneous network setting where it co-exists with a ZP-OFDM communication link, then in a homogeneous network setting where all links are using MCSS scheme.

KEYWORDS

Software-defined Networks, Multi-Dimensional Chirp Spread Spectrum, Coexistence, Heterogeneous Networks.

ACM Reference Format:
Kerem Enhos, Emrecan Demirors, Deniz Unal, Tommaso Melodia. 2022. Coexistence of Multi-Dimensional Chirp Spread Spectrum in Underwater Acoustic Networks. In *The 16th International Conference on Underwater Networks & Systems, November 14-16, 2022, Boston, MA.* ACM, New York, NY, USA, 8 pages.

1 INTRODUCTION

Underwater acoustic networks are increasingly becoming popular, thanks to the many applications they play a vital role in. Offshore equipment and infrastructure monitoring, fisheries and aquaculture, and unmanned underwater vehicles are only some of these applications. The widespread adoption of underwater networks will impose a significant burden on already scarce underwater acoustic spectrum resources.

Underwater acoustic spectrum is inherently scarce, mainly due to the frequency and range-dependent high path loss. To be more specific, underwater acoustic devices operating over long-range links (i.e., 10 - 100 km) may have available bandwidths of only a few kHz, while devices operating over medium-range links (i.e., 1 - 10 km) and short-range links (i.e., 0.1 - 1 km) have available bandwidths of on the order of 10 kHz and few tens of kHz, respectively. Only devices operating over very short-range links (less than 100 m) may have more than 100 kHz bandwidth [11]. Temporal and spatial variations of channel coefficients, colored noise, multipath effect, and Doppler effect are additional factors further limiting underwater spectrum resources.

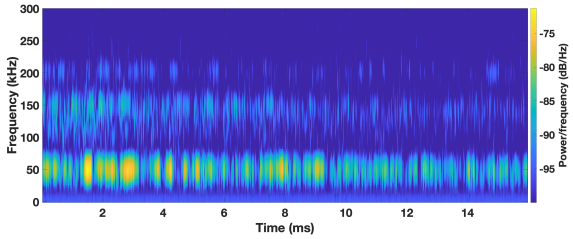

Figure 1: Recorded underwater acoustic spectrum of the Boston Harbor.

Underwater acoustic spectrum is not regulated or standardized. Unlike the RF spectrum, underwater communication devices do not require licenses to operate at certain spectrum bands, which means they can use any portion or even the entire spectrum at any time. Moreover, communication devices are not the only man-made systems using the underwater spectrum. Passive and active SONAR systems used in applications like seismology, profiling, exploration, and navigation also occupy parts of the underwater spectrum. Furthermore, some marine animals can potentially use spectrum resources. To provide a real-world example, we have recorded the acoustic spectrum (at frequencies from 0 to 300 kHz) of the Boston Harbor in a time period when shipping and boating activity is relatively low. Figure 1 depicts a snapshot from this recording, which offers valuable insight into the underwater spectrum usage. Particularly, it proves even at a location where no known underwater network deployments, the underwater acoustic spectrum could be heavily occupied.

There have been significant efforts to solve this, so-called *spectrum crunch* in the over-the-air networking domains [1, 14]. Most of these solutions are essentially leveraging spectrum-sharing strategies based on mutual temporal exclusion, which means only one wireless system is allowed to use a channel medium at each time instant, while other systems need to stay silent. However, this approach is not applicable in underwater acoustic communication due to the high and variable propagation delay. On the other hand, solutions based on time division multiple access (TDMA) can offer only limited channel utilization efficiency in large-scale networks since they require long-time guards and/or heavy signaling requirements for underwater acoustic sensor networks.

WUWNet'22, November 14-16, 2022, Boston, MA

To address the underwater *spectrum crunch*, in this paper, we propose Multi-Dimensional Chirp Spread Spectrum (MCSS). MCSS is a code-time-frequency multidimensional spreading scheme, which enables communication in heterogenous networks under the influence of different levels of interference and noise. By using these physical layer scheme, successful communication links can be utilized within both existing heterogeneous networks or homogeneous networks that also use the MCSS scheme. Thus, with the MCSS scheme, zero signaling exchange among the coexisting technologies can be utilized, and modification to the protocol stack for previously deployed systems is not required.

In this paper, we first describe the proposed MCSS scheme in Section 2. Then, testbed, hardware and software architecture that is used throughout the experiments are described in Section 3. In Section 4, we provide comprehensive experimental performance evaluation of MCSS in both heterogeneous and homogeneous underwater acoustic networks. Finally, concluding remarks are given in Section 5.

2 MULTI-DIMENSIONAL CHIRP SPREAD SPECTRUM SCHEME

Multi-Dimensional Chirp Spread Spectrum (MCSS) scheme is first presented in [5] as chirp-based *low probability of detection and low probability of interception (LPD/LPI)* with code-time-frequency multidimensional spreading scheme. MCSS provides robust communication using chirp-based acoustic pulses that combines spreading codes with frequency and time hopping patterns as shown in Fig. 2. For each transmission of MCSS, different patterns, which consists number of frames, that includes spread-spectrum encoded chirp-based ultrasonic pulses within different time slots and frequency bins, are associated with individual users. MCSS enables receiver performance that is robust and resilient against severe channel effects. Due to it's spread spectrum characteristics, probability of detection by any unintended user is also lower. Thus, such coding pattern provides (i) *low probability of recognition or detection by an adversary* and (ii) *robust detection in adverse channels with the frequency-time hopping pattern and spreading code that is known to the intended receiver.*

First, MCSS's robust reception and demodulation performance under low signal-to-noise ratio (SNR) condition reduces the need for high transmission power. By increasing the processing gain (time-bandwidth product), reception performance and resilience against severe channel effects, such as multipath, scattering, and Doppler effect [10] can be improved. Second, probability of interception and detection is lower since chirp signals are wideband signals and have low power spectral density at a given SNR level. Third, ubiquitous nature and presence of chirp signals in the underwater environment (e.g., dolphin clicks [2, 8]) decreases the probability of detection due to the difficulty of associating these pulses with particular communication methods. Last, chirps can be generated with minimal signal processing, and data rate can be arbitrarily exchanged for power spectral density and communication distance.

Due to their (i) *low computational complexity* and (ii) *inherent robustness to multipath*, pseudo-orthogonal spreading codes are used to represent each information bit in the proposed method [7, 9, 12]. A chirp signal is defined by a time-varying instantaneous

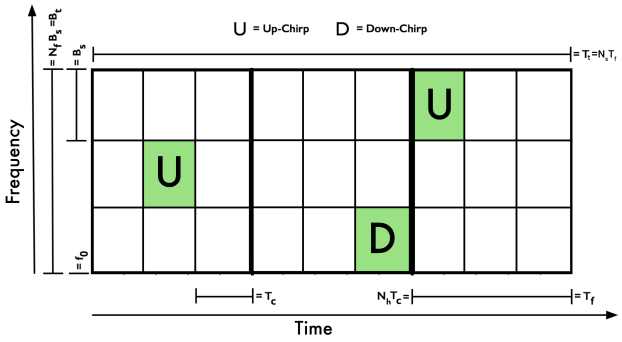

Figure 2: An example of a $M_s(3,3,3)$ MCSS frame transmission with frequency hopping, time hopping, and spreading code lengths of 3, 3, and 3 respectively. Frequency-hopping sequence $FH = \{2,1,3\}$ time-hopping sequence $TH = \{2,3,1\}$, and spreading code sequence $SC = \{1,-1,1\}$ sending information bit 1.

frequency that shifts with time from an initial value of f_0 to a final value of f_1, where the total bandwidth of the chirp is defined as $B_s = f_1 - f_0$. By utilizing the quasi-orthogonality of up and down chirps and encoding a "1" information symbol with an up-chirp and a "-1" information symbol with a down-chirp, the train of chirps, which time-domain expression is given in [5], can be modulated based on binary orthogonal keying (BOK). Since the information bit in BOK-spreading is distributed using BOK-modulated chips, the pseudo-orthogonal spreading code can be characterized as pseudorandom code of N_s chips with $a_j \in \{-1, 1\}$.

For MCSS a consolidated code spreading, frequency and time hopping method can be considered, as shown in Fig. 2. This method divides the frequency spectrum B_t into N_f sub-bands of bandwidth B_s as well as the slotted time into chips of duration T_c, with the chips organized into frames of duration $T_f = N_h \cdot T_c$, where N_h is the number of chips per frame. Different time hopping sequences (TH), frequency hopping sequences (FH), and spreading code sequences (SC) are assigned to individual users and chirp signals corresponding to each pre-defined sequence is transmitted for each information bit. Pseudo-random sequences produced by seeding random number generators serve as the foundation for both time-frequency hopping and spreading code sequences. Thus, MCSS frame signal can be expressed by $s(t,i)$ for i^{th} information bit with frequency and time hopping and BOK-spreading as

$$\hat{t} = \left(t - c_j T_c - j T_f\right), \tag{1}$$

$$s(t,i) = \sum_{j=0}^{N_s-1} \cos\left(2\pi f_{k_j}\hat{t} + \left(1 - \left(a_j d_i\right)\right)\pi B_s \hat{t} + \left(a_j d_i\right)\pi\mu\hat{t}^2\right), \quad 0 \le \hat{t} \le T_c, \tag{2}$$

where $\mu = \frac{B_s}{T_c}$, $\{c_j\}$ is the time hopping sequence, with $0 \le c_j \le N_h - 1$, $\{k_j\}$ is the frequency hopping sequence with $0 \le k_j \le N_f - 1$, and $\{d_i\}$ is the information bits where $d_i \in \{-1, 1\}$. Since MCSS frame is associated with N_s chips represents one information bit, the corresponding data rate can be expressed as

$$R(N_h, N_s) = \frac{1}{N_s T_f} = \frac{1}{N_s N_h T_c}, \tag{3}$$

where the trade off between the communication robustness, resilience to noise and multipath (by increasing the number of chips or chirp duration) and energy per bit, data rate can be observed with (3).

In BOK-spreading, the receiver demodulates the information bits by using the correlation result with the spreading code used at the transmitter. It is crucial to note that for BOK scheme a conventional non-coherent energy detector receiver is sufficient, in contrast to binary phase shift keying (BPSK) modulated signals, which require a coherent receiver with precise channel information for decoding. Former scheme only requires frame synchronization and has a lower complexity of implementation.

As mentioned previously, extending the spreading code used in the MCSS frame by either using longer chirp duration, T_c, or increasing the number of chips, N_s, leads to more robust communication link performance due to the inducement of higher processing gain. Signal-to-interference-plus-noise ratio (SINR) at the receiver can be expressed as

$$SINR_{init} = \frac{Pg}{I + \eta}, \tag{4}$$

where, P is the transmitted signal power, g is the path gain, I is the received interference power and η is the noise power level at the receiver. Chirp signals provide a processing gain proportional to the time-bandwidth product (TB), resulting in improved SNR at the receiver following the signal processing. Contrary to narrowband pulses, the duration T_c and bandwidth B_s of chirp signals can be differentiated separately to provide higher processing gain, which can be expressed as [10]

$$PG = \frac{T_c B_s}{0.886}, \tag{5}$$

After including frequency, time and chip spreading to the chirp transmission, processing gain is increased for MCSS transmission and SINR at the receiver can be rewritten by using (4) as [5, 15, 16]

$$SINR_{rec}(N_f, N_h, N_s) = \left(\frac{T_c B_s N_f N_h N_s}{0.886}\right) SINR_{init}, \tag{6}$$

By (6) and (3), it can be observed that processing gain can be increased with the drawback of decreased data rate. On the other hand, increasing the bandwidth of the chirp signal, B_s, increases the processing gain without affecting the data rate. However, in bandwidth limited applications, where utilized bandwidth of the transmitted chirp should be kept constant or within a limited range, data rate can only be increased by decreasing the processing gain, which can be enabled by decreasing the chirp duration or number of chips, frequency bins, and chips per frame. For the latter option data rate can be maximized by implementing binary chirp spread spectrum. However, while using MCSS scheme, data rate can be increased by reducing the chirp length, which is limited by applicable processing gain. Decreasing the processing gain can lead to lower probability of detection of MCSS frames and consequently increased BER. With known or estimated noise and interference levels, resulting bit error rate (BER) can also be approximated using (6).

3 TESTBED, HARDWARE AND SOFTWARE

In this section, we introduce the underwater acoustic communication modem, testbed and the software framework that is used throughout the experiments.

Testbed: Experiments are conducted at Charlestown Marina in Boston, Massachusetts. We deployed four software-defined acoustic modems in pairs approximately 10 meters apart from each other. Each pair deployed as one modem's transducer facing towards the sea bottom and 1 meter depth and the other modem's transducer facing towards the sea surface with approximately 11 meter depth, forming a vertical channel between two modems. Each modem is connected to a network switch, which is also connected to a mini-PC. Internet connection to the mini-PC is provided by a LTE modem, which enables the user to have secure shell connection to the modems. File transfer, different communication scheme executions and data recording operations are conducted through remote connection.

Hardware: Throughout the experiments, we used SEANet modems [3, 6], which can operate at a wide range of acoustic frequencies by using software-defined radio (SDR) paradigm, which enables us to use several different physical layer schemes, simultaneously and interchangeably. In our experiments, SEANet modems are coupled with a transmitting transducer that has 200 kHz bandwidth with 145 kHz resonance frequency and as the receiver, a hydrophone is used, which has a flat frequency response with 200 kHz bandwidth centered at 100 kHz. Due to its configurable nature, transmitting and receiving gain can be adjusted digitally through a remote connection and throughout the experiments, the signal level is adjusted by differentiating the transmission gain digitally. Each modem has both transmission and reception capabilities, thus they can be used bi-directionally or interchangeably. Detailed hardware architecture is given in [3].

Software: By leveraging SEANet modem's software-defined architecture, physical layers are generated for both ZP-OFDM and Multi-Dimensional Chirp Spread Spectrum (MCSS) transmitter and receiver signal processing chains. For the ZP-OFDM communication scheme, packets are generated as defined in Section 4, with randomly generated binary data and delivers the desired waveform to the DAC to be transmitted through the acoustic transducer. For the receiver chain, signal received and amplified from the hydrophone is converted to digital domain to conduct packet detection, by using cross-correlation of pseudo randomly generated preamble. After successful packet detection and demuxing stages, OFDM signal is equalized by using its corresponding pilot subcarriers. Following the equalization step, QAM demodulation is conducted and resulting binary bits are compared with the transmitted bits to calculate the bit-error-rate of the communication link at different signal and interference levels. For signal-to-noise (SNR) and signal-to-interference-plus-noise (SINR) ratio calculations, further observation and signal processing purposes, transmitted acoustic waveforms are recorded and processed offline.

As for the MCSS scheme, transmitted waveforms can be generated with desired number of frequency bins, time-hopping sequence

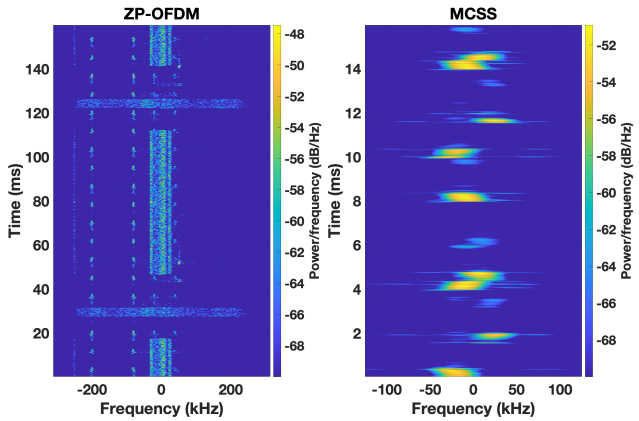

Figure 3: Spectrogram of the received baseband ZP-OFDM (left) and MCSS (right) signals.

and spreading codes. SDR paradigm enables easy implementation and real-time adjustments of different chirp lengths, utilized bandwidth, hopping and spreading sets and center frequency. Similarly, on the receiver chain, packet detection is conducted with the cross-correlation of a preamble generated again with MCSS scheme with a much longer spreading code compared to data signal. After successful packet detection, each bit is obtained by cross-correlation of each chirp spreading set with the received signal.

4 PERFORMANCE EVALUATION

As described in Section 1, underwater acoustic communication systems are lacking conventional communication standards unlike the RF domain. Thus, underwater communication systems deployed over a vast area need to operate and have the capability to utilize successful communication links in heterogeneous networks. In this section, we present two different set of experiments to investigate the coexistence of MCSS scheme in heterogeneous networks. The first set of experiments are conducted with using Zero-Padded OFDM (ZP-OFDM) and as the second set Turbo encoded ZP-OFDM is used as the physical layer that is investigated for the coexistence of MCSS. Similarly, performance of the MCSS links implemented in a centralized homogeneous network structure is also showcased.

Specifically ZP-OFDM is selected for the investigation of performance of MCSS in heterogeneous networks since it is a well known PHY layer in RF domain standards as well as it is a widely used and researched communication scheme that is used as an underwater acoustic communication method. Because of it's spectral efficiency, multi-path resilience and high data rate capability, ZP-OFDM is a great candidate for future underwater acoustic communication network systems and standards [4, 13]. Thus, coexistence of the proposed communication scheme with ZP-OFDM is vital in order to have robust links with high interference or to increase data rate with cooperative transmission in heterogeneous communication systems.

Throughout the experiments, ZP-OFDM is generated by using 8192 subcarriers over 125 kHz of bandwidth, where 1024 of these are used as pilot subcarriers and 3072 data subcarriers. Remaining subcarriers are used as null, which are allocated at sidebands.

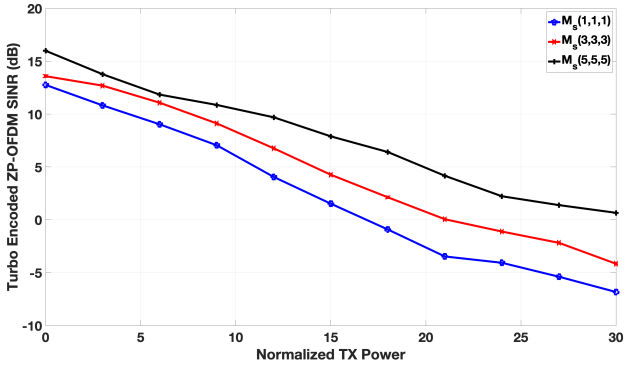

Figure 4: SINR level obtained at the ZP-OFDM receiver with different MCSS transmission gain.

Thus, only 62.5 kHz bandwidth is allocated by the data and pilot subcarriers centered around DC as the waveform is generated in baseband. Each OFDM symbol is prepended with pseduo-randomly generated preamble of approximately 4 μs duration followed by a guard interval of 15 milliseconds. After each OFDM symbol, a pause interval of 10 milliseconds is appended to form the ZP-OFDM packet [4]. After packet detection of preamble, signal is demuxed and channel estimation is conducted to be used for zero forcing spectrum equalization. After the equalization step, demodulated binary bits are compared with the transmitted binary bits to obtain BER of ZP-OFDM.

A similar packet structure is used for MCSS scheme, where instead of a pn-sequence preamble, another distinct MCSS frame is used as preamble. MCSS preamble is formed with 30 spreading frames and randomly generated frequency/time-hopping and coding patterns. Although such long frame durations are not needed for successful communication links, in order to avoid misdetection of packets processing gain is increased arbitrarily for the preamble. For the data frames, again each bit is obtained by randomly generated frequency/time-hopping and coding sequence, which can represented as $M_s(N_f, N_h, N_s) = [(FH), (TH), (SC)]$, where $M_s(N_f, N_h, N_s)$ is the MCSS sequence, FH, TH, and SC are the frequency hopping, time hopping and coding sequences respectively.

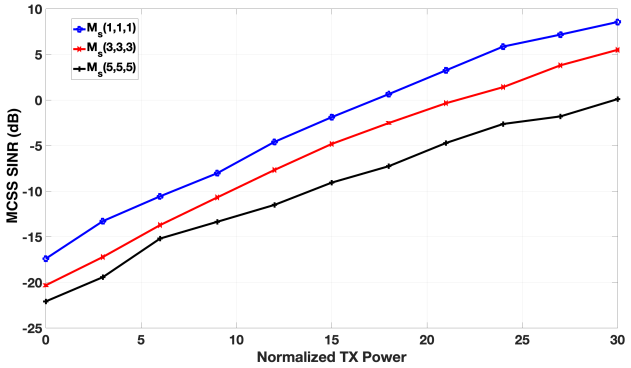

Figure 5: SINR level obtained at the MCSS receiver with different MCSS transmission gain, while having constant ZP-OFDM transmission gain.

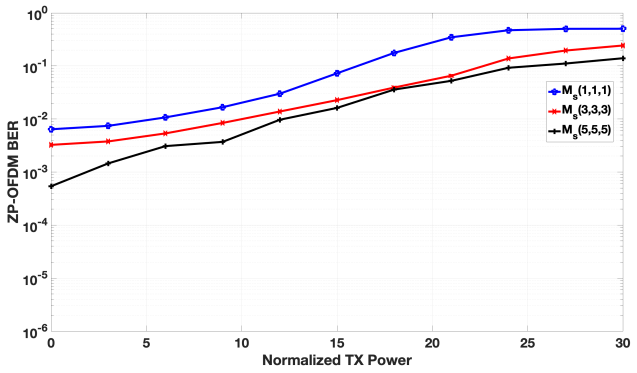

Figure 6: BER of ZP-OFDM reception with different MCSS transmission gain, while having constant ZP-OFDM transmission gain.

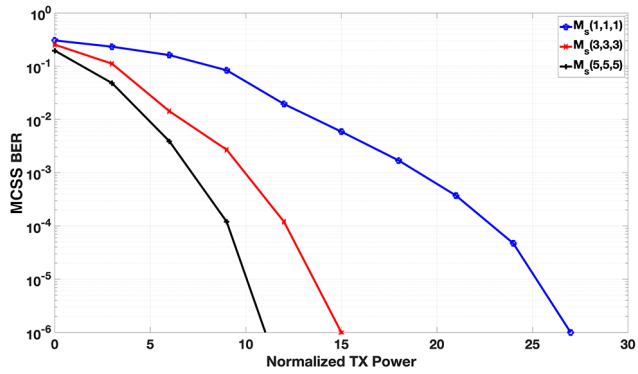

Figure 7: BER of MCSS reception with different MCSS transmission gain, while having constant ZP-OFDM transmission gain.

For experiments conducted in Section 4.1 and 4.2, *Modem 1* is used as the MCSS transmitter and it's corresponding sequence is shown in Table 1. For other transmitter modems used in Section 4.3, MCSS sequences are also given in Table 1. Though, these patterns are representing bit 1, inverse of coding sequence resembles bit 0, hence frequency and time hopping sequences are same for each bit but coding sequences are changed by converting upchirp to downchirp.

In this paper three different MCSS sequences, $M_S(1,1,1)$, $M_S(3,3,3)$, and $M_S(5,5,5)$, are observed. The sequence of $M_S(1,1,1)$, corresponds to binary chirp spread spectrum transmission, which has higher spectral efficiency but worse BER performance. Throughout the experiments, 10 kHz of bandwidth for each frequency bin is utilized for MCSS sequences and total utilized bandwidth is kept within the bandwidth of ZP-OFDM. Another important parameter for MCSS sequence is the chirp duration, which is also used for number time hopping intervals. In each experiment, chirp duration is selected to be 400 μs. With these parameters corresponding data rates are 4166, 463, and 167 bps with processing gains of 4.51, 40.63, and 564.33 for MCSS sequences, $M_S(1,1,1)$, $M_S(3,3,3)$, and $M_S(5,5,5)$ respectively. For both modulation schemes, transmitted waveforms are generated at baseband and upmixed to 140 kHz center frequency to be transmitted in passband. At the receiver chain, received signal is downmixed again to baseband for demodulation signal processing as can be seen in the spectrogram given in Fig. 3.

In order to investigate the coexistence of MCSS and ZP-OFDM, one pair of modems that form a vertical channel is used to maintain ZP-OFDM communication link while other pair that is 10 meter apart is used to utilize MCSS scheme as described in Section 3. During the experiments transmission gain of ZP-OFDM is kept constant, where SNR level of 22 dB can be obtained without any interference and transmission gain of MCSS scheme is differentiated. Hence, SNR level of ZP-OFDM transmission is kept constant and interference level is increased, which lowers the SINR level, by increasing the transmission gain of the MCSS scheme. In Fig. 4, SINR level of the ZP-OFDM receiver is shown for different transmission gain levels of the MCSS transmitter. Similarly, SINR level of MCSS is measured with constant ZP-OFDM transmission gain, which is shown in Fig. 5 for different transmission gain levels of the MCSS transmitter. In order to have a better visualization and more fair comparison of different spreading of MCSS, which leads to different transmission power, bit-error-rate of the proposed MCSS and ZP-OFDM physical layers are illustrated with respect to the transmission gain level of the MCSS in the following sections.

4.1 Coexistence of MCSS with ZP-OFDM

Firstly, coexistence of MCSS with ZP-OFDM is investigated. With the ZP-OFDM scheme, 31 kbps can be achieved by utilizing 62.5 kHz bandwidth and BPSK modulated OFDM symbols with 4096 allocated subcarriers, where 1024 subcarriers are used as pilot for equalization. As it is shown in Fig. 6 MCSS has great impact on ZP-OFDM, where BER increases over 10^{-3} for SINR levels of 15 dB. Since ZP-OFDM gets affected by any other signal in the same bandwidth, chirp signals causes inaccurate channel estimation that is used for the zero forcing equalization of OFDM signal, which disrupts successful communication.

However, SINR levels higher than -12 dB for MCSS scheme, BER results in lower than 10^{-6}, which shows that even though ZP-OFDM is adversely affected by the presence of MCSS in the same network area, MCSS can still accomplish successful communication under the presence of ZP-OFDM signaling. As shown in Fig. 7, as the spreading sequence increases, lower BER can be obtained at lower SINR.

4.2 Coexistence of MCSS with Turbo Encoded ZP-OFDM

As shown in Section 4.1, MCSS transmission adversely affect ZP-OFDM communication link even for low interference levels. In order to achieve successful communication for the ZP-OFDM scheme, one conventional solution that is widely used is utilizing error-coding schemes such as Turbo encoding. With the Turbo encoding, data rate decreases by three times with the 1/3 rate Turbo encoding to 10.31 kbps. Although data rate gets impacted by the error coding, it also solves the inaccurate channel estimation and equalization problem with the interleaved data subcarrier structure.

In Fig. 8, it is shown that BER of lower than 10^{-6} can be achieved for SINR levels higher than 7 dB for Turbo encoded ZP-OFDM in a

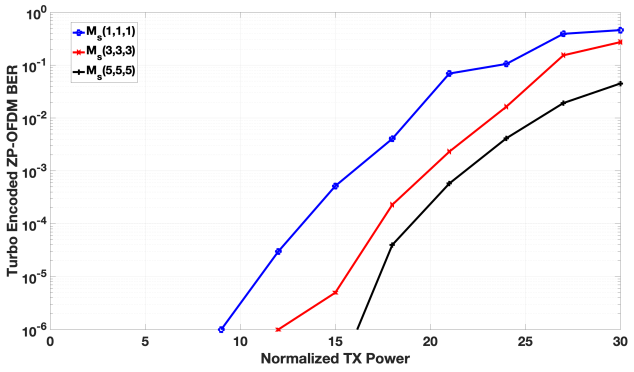

Figure 8: BER of Turbo encoded ZP-OFDM reception with different MCSS transmission gain, while having constant ZP-OFDM transmission gain.

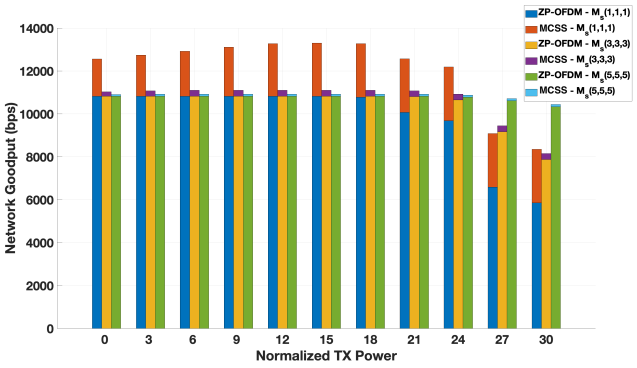

Figure 9: Total network goodput of ZP-OFDM and MCSS schemes for different transmission gain levels of MCSS, with constant ZP-OFDM transmission gain.

heterogeneous network consisting MCSS nodes, which is a great improvement compared to ZP-OFDM without error coding.

After observing that Turbo encoded ZP-OFDM and MCSS can coexist at appropriate transmission gain levels, total network goodput is assessed in Fig. 9. It can be seen that since data rate of ZP-OFDM is much higher than MCSS, network goodput cannot be increased in a cooperative communication method manner. However, both physical layers can coexist at certain transmission power levels, which can be seen as the total network goodput increases. Also for high interference levels of MCSS, ZP-OFDM goodput decreases rapidly, but it can be observed that as the spreading of MCSS increases, impact of interference on the ZP-OFDM goodput decreases and even with the very low contribution of MCSS on the total network goodput, ability to coexist results in higher goodput compared to MCSS spreading that can achieve high data rate. However, as shown in Fig. 10, even though coexistence can be achieved and higher goodput can be achieved as spreading increases, energy per bit also increases. Thus, with the drawback of higher energy consumption, MCSS and other physical layers can coexist and goodput can be increased.

4.3 Centralized Homogeneous MCSS Network

After investigating the coexistence of MCSS in heterogeneous networks, coexistence of MCSS under the interference of other transmitters using MCSS scheme in a homogeneous network manner is also observed. Diversely from the previous experiments, instead of one pair of modems over a vertical channel, only one of the modems that is deployed at 1 meter depth with it's transducer facing towards the sea bottom is used as the receiver and all other three modems are used as MCSS transmitters. For observing the coexistence of MCSS with different randomly generated MCSS signal interference, transmitter modem that forms a vertical channel with the receiver is used as the primary source of transmission and other transmitter modems are used as interference sources. Thus, the transmission gain of interference sources are kept constant and signal level is differentiated by using the primary transmitter modem. As applied previously, similar approach is conducted to calculate the SINR level at the receiver by differentiating the transmission gain of the primary transmitter modem as shown in Fig. 11.

Following the SINR measurements, BER performance of MCSS scheme under interference of two different MCSS transmitters is characterized as given in Fig. 12. It can be seen that for MCSS frame structure of $M_s(1,1,1)$ acts as vast interference source and probability of packet detection and demodulation is decreased. As proposed for MCSS scheme, it is shown that applying a multi-dimensional

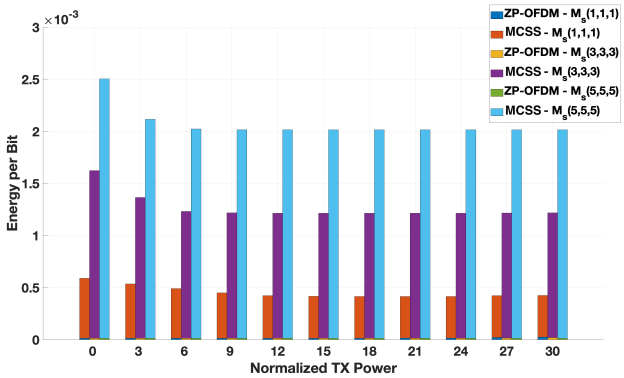

Figure 10: Energy per bit for ZP-OFDM and MCSS schemes for different transmission gain levels of MCSS, with constant ZP-OFDM transmission gain.

Modem #	$M_s(1,1,1)$	$M_s(3,3,3)$	$M_s(5,5,5)$
1	[(1),(1),(1)]	[(2,1,3), (2,3,3), (1,1,1)]	[(2,1,5,2,4), (5,5,4,5,1), (1,-1,1,1,-1)]
2	[(1),(1),(-1)]	[(2,3,1), (2,3,3), (-1,-1,-1)]	[(3,4,2,3,5), (5,1,2,1,3), (-1,-1,1,-1,1)]
3	[(1),(1),(1)]	[(3,3,2), (3,1,1), (-1,-1,-1)]	[(5,5,4,4,1), (1,2,2,1,1), (1,1,-1,1,-1)]

Table 1: MCSS frame sequences resembling bit 1 used by each transmitter modem with different frame lengths.

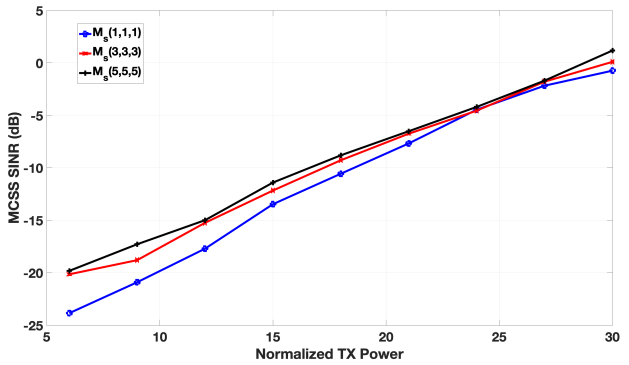

Figure 11: SINR level at the receiver modem by differentiating the transmission gain of the primary transmitter while keeping other two interference sources' transmission gains constant.

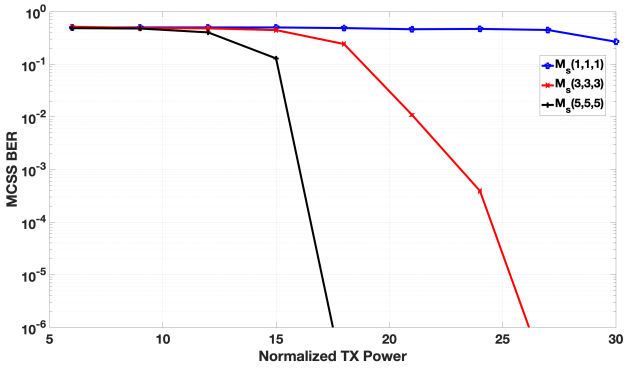

Figure 12: BER of the primary transmitter at different transmission gains while keeping other two interference sources' transmission gains constant.

hopping structure enables successful communication link under strong interference and low signal levels. For both $M_s(3,3,3)$ and $M_s(5,5,5)$ MCSS frame structure BER performance lower than 10^{-6} can be obtained for SINR levels lower than -3 dB, which infers to the fact that MCSS scheme can enable robust communication for signal levels lower than noise and interference levels.

As a final observation case, it is realized that MCSS can also be used in a centralized network structure. This means that several asynchronous transmitters can be simultaneously used to communicate with a single receiver structured as a centralized network. This capability is substantially important for underwater acoustic communication, which lacks of any standardized MAC layer. Also majority of MAC protocols require timing synchronization or feedback mechanism to avoid collision and efficient communication structure, which is a huge disadvantage for the communication domain of underwater acoustics that has vast delay spread and propagation delay.

Although, this centralized structure eliminates the need for a MAC protocol, it can also be used as a cooperative communication scheme to increase data rate by increasing the number of transmitting nodes. Asynchronous spread spectrum transmission with different channels and nodes can be demodulated to assemble and obtain more data without any time loss between switching of different transmitters or packet detection.

Since each transmitter has a different channel structure and distance to the receiver modem, for a fair comparison, each transmitter modem's transmission gain is adjusted to obtain 0 dB SNR level at the receiver modem without any interference source. After this adjustment, randomly generated MCSS frame structures of $M_s(3,3,3)$ and $M_s(5,5,5)$ with different randomly generated binary bits are transmitted and received from a single receiver source to be demodulated. Due to its low probability of interception nature, each transmitter's packets can be detected individually and decoding of binary bits are accomplished under constant interference, noise and signal levels. It is can be seen from the Fig. 13, that increasing the number of frequency/time-hopping sequence and coding frame length, decreases the BER with the degradation on the data rate and at the expense of higher energy per bit. Apart from the MCSS frame structure comparison, chirp duration of each MCSS frame is differentiated to observe the effect of chirp duration on the demodulation performance and also the limits of coexistence, demodulation and interference levels in a centralized homogeneous MCSS network structure. As it is shown in Fig. 13, as the chirp duration increases, bit error probability decreases due to the fact that cross-correlation of MCSS frames with longer chirp duration acquires easier detection of binary bits (or MCSS frames) at the expense of lower data rate.

5 CONCLUSIONS AND FUTURE WORK

We proposed MCSS scheme, enabling robust and efficient communication in heterogeneous underwater acoustic networks without degrading the communication performance of the coexisting unregulated physical layers. First we described the communication scheme that uses code-time-frequency multidimensional spreading and how it benefits the receiving performance of the communication link. Then, we demonstrated the experimental performance of MCSS in a heterogeneous network consisting ZP-OFDM in the communcation channel. Moreover, we demonstrated the feasibility

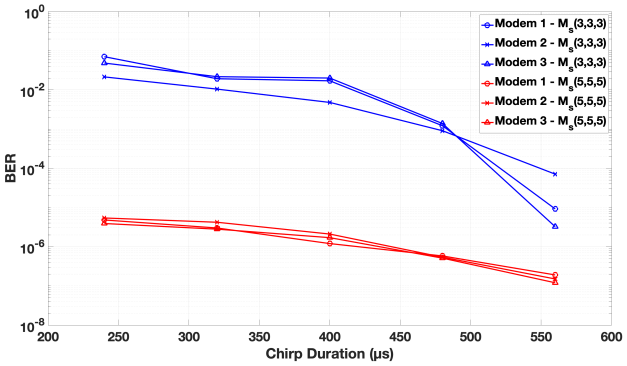

Figure 13: BER of each modem for MCSS frame structures of $M_s(3,3,3)$ and $M_s(5,5,5)$.

of using MCSS in a homogeneous network where multiple transmitters are used to communicate with a centralized receiver node and the affect of the interference of different transmitters on the communication link. As future work, we are planning to fully explore the communication performance of MCSS in different channel configurations to formulate a generalized expression. By such mathematical modeling, an optimized and adaptive software-defined communication system can be implemented, which can reconfigure it's physical layer parameters according to the estimated channel properties.

REFERENCES

[1] Lorenzo Bertizzolo, Emrecan Demirors, Zhangyu Guan, and Tommaso Melodia. 2020. CoBeam: Beamforming-based Spectrum Sharing With Zero Cross-Technology Signaling for 5G Wireless Networks. In *Proc. of IEEE Conference on Computer Communications (INFOCOM)*. 1429–1438.

[2] Chris Capus, Yan Pailhas, Keith Brown, David M. Lane, Patrick W. Moore, and Dorian Houser. 2007. Bio-inspired wideband sonar signals based on observations of the bottlenose dolphin (Tursiops truncatus). *The Journal of the Acoustical Society of America* 121, 1 (2007), 594–604. https://doi.org/10.1121/1.2382344 arXiv:https://doi.org/10.1121/1.2382344

[3] E. Demirors, J. Shi, A. Duong, N. Dave, R. Guida, B. Herrera, F. Pop, G. Chenand C. Casella, S. Tadayon, M. Rinaldi, S. Basagni, M. Stojanovic, and T. Melodia. 2018. The SEANet Project: Toward a Programmable Internet of Underwater Things. In *Proc. of IEEE Underwater Communications Conf. And Workshop (UComms)*. Lerici, Italy.

[4] E. Demirors, G. Sklivanitis, G. E. Santagati, T. Melodia, and S. N. Batalama. 2018. A High-Rate Software-Defined Underwater Acoustic Modem With Real-Time Adaptation Capabilities. *IEEE Access* 6 (2018), 18602–18615.

[5] E. Demirors and T. Melodia. 2016. Chirp-Based LPD/LPI Underwater Acoustic Communications with Code-Time-Frequency Multidimensional Spreading. In *Proc. of ACM Intl. Conf. on Underwater Networks & Systems (WUWNet)*. Shanghai, China.

[6] E. Demirors, J. Shi, R. Guida and T. Melodia. 2016. SEANet G2: A Toward a High-Data-Rate Software-Defined Underwater Acoustic Networking Platform. In *Proc. of ACM Intl. Conf. on Underwater Networks & Systems (WUWNet)*. Shanghai, China.

[7] Kanke Gao, Lei Ding, Tommaso Melodia, Stella N. Batalama, Dimitris A. Pados, and John D. Matyjas. 2011. Spread-spectrum cognitive networking: Distributed channelization and routing. In *2011 - MILCOM 2011 Military Communications Conference*. 1250–1255. https://doi.org/10.1109/MILCOM.2011.6127472

[8] D. S. Houser, D. A. Helweg, and P. W. Moore. 1999. Classification of dolphin echolocation clicks by energy and frequency distributions. *The Journal of the Acoustical Society of America* 106, 3 (1999), 1579–1585. https://doi.org/10.1121/1.427153 arXiv:https://doi.org/10.1121/1.427153

[9] Ming Li, Stella N. Batalama, Dimitris A. Pados, Tommaso Melodia, Michael J. Medley, and John D. Matyjas. 2011. Cognitive Code-Division Links with Blind Primary-System Identification. *IEEE Transactions on Wireless Communications* 10, 11 (2011), 3743–3753. https://doi.org/10.1109/TWC.2011.091911.101260

[10] X. Lurton. 2002. *An Introduction to Underwater Acoustics: Principles and Applications*. Springer. https://books.google.com.tr/books?id=VTNRh3pyCyMC

[11] T. Melodia, H. Kulhandjian, L. Kuo, and E. Demirors. 2013. Advances in Underwater Acoustic Networking. In *Mobile Ad Hoc Networking: Cutting Edge Directions* (2nd ed.), S. Basagni, M. Conti, S. Giordano, and I. Stojmenovic (Eds.). John Wiley and Sons, Inc., Hoboken, NJ, 804–852.

[12] Dario Pompili, Tommaso Melodia, and Ian F. Akyildiz. 2009. A CDMA-based Medium Access Control for UnderWater Acoustic Sensor Networks. *IEEE Transactions on Wireless Communications* 8, 4 (2009), 1899–1909. https://doi.org/10.1109/TWC.2009.080195

[13] Andreja Radosevic, Rameez Ahmed, Tolga M. Duman, John G. Proakis, and Milica Stojanovic. 2014. Adaptive OFDM Modulation for Underwater Acoustic Communications: Design Considerations and Experimental Results. *IEEE Journal of Oceanic Engineering* 39, 2 (2014), 357–370. https://doi.org/10.1109/JOE.2013.2253212

[14] Jonathan Rodriguez. 2014. *The Wireless Spectrum Crunch*. 165–189. https://doi.org/10.1002/9781118867464.ch7

[15] G. Enrico Santagati, Tommaso Melodia, Laura Galluccio, and Sergio Palazzo. 2015. Medium Access Control and Rate Adaptation for Ultrasonic Intrabody Sensor Networks. *IEEE/ACM Transactions on Networking* 23, 4 (2015), 1121–1134. https://doi.org/10.1109/TNET.2014.2316675

[16] M.Z. Win and R.A. Scholtz. 2000. Ultra-wide bandwidth time-hopping spread-spectrum impulse radio for wireless multiple-access communications. *IEEE Transactions on Communications* 48, 4 (2000), 679–689. https://doi.org/10.1109/26.843135